Compensation of charging in X-PEEM: a successful test on mineral inclusions in 4.4 Ga old zircon

Gelsomina De Stasio[a,*], Bradley H. Frazer[a,b], Benjamin Gilbert[c],
Katherine L. Richter[d], John W. Valley[e]

[a] *Department of Physics and Synchrotron Radiation Center, University of Wisconsin–Madison, 3731 Schneider Drive,
Stoughton WI 53589, USA*
[b] *Institute de Physique Appliquée, Ecole Polytechnique Fédérale de Lausanne, CH-1015 Lausanne, Switzerland*
[c] *Earth and Planetary Science, University of California-Berkeley, Berkeley CA 94720, USA*
[d] *Bob Jones University, Greenville SC 29614, USA*
[e] *Department of Geology and Geophysics, University of Wisconsin, Madison WI 53706, USA*

Abstract

We present a new differential-thickness coating technique to analyze insulating samples with X-ray PhotoElectron Emission spectroMicroscopy (X-PEEM). X-PEEM is non-destructive, analyzes the chemical composition and crystal structure of minerals and can spatially resolve chemical species with a resolution presently reaching 35 nm. We tested the differential coating by analyzing a 4.4 billion-year-old zircon ($ZrSiO_4$) containing silicate inclusions. We observed quartz (SiO_2) inclusions smaller than 1 μm in size that can only be analyzed non-destructively with synchrotron spectromicroscopies. With the removal of charging we greatly extend the range of samples that can be analyzed by X-PEEM.

1. Introduction

X-ray PhotoElectron Emission spectroMicroscopy (X-PEEM) has proven to be a powerful technique for the microchemical analysis of conductors or thin biological specimens [1–5]. Briefly, in this type of microscopy a flat, conductive sample is illuminated by monochromatic soft-X-rays (10–2000 eV) from a synchrotron beamline, and electron emission occurs by the photoelectric effect. A high negative voltage applied to the sample accelerates photoelectrons into an electron optics system, to produce a real-time, magnified image of the sample surface. The majority of the signal in X-PEEM images originates from secondary electrons. While other spectromicroscopies

---

*Corresponding author. Tel.: +1-608-877-2000; fax: +1-608-877-2001.

E-mail address: pupa@src.wisc.edu (G. De Stasio).

based on microfocusing and fluorescence offer similar capabilities [6,7], X-PEEM is unique in several regards. It is a full field, real-time imaging system that may be easily moved and installed on different beamlines. The photon energy range and spectral resolution are therefore limited only by the choice of beamline. Microfocusing fluorescence spectromicroscopies have the advantage of working at air pressure, but the intense photon flux at the focus location can prove destructive on most samples.

Microchemical information is obtained by scanning the energy of the monochromatic X-rays across the absorption edges of selected elements. In this way, X-ray absorption near edge structure (XANES) information is acquired for each image pixel. In practice, one image at each photon energy is acquired and stored in a stack of images, or ''movie'', as the energy is scanned. XANES spectra associated with any surface region can be extracted from the movies immediately or off-line, away from the source.

XANES spectra carry information on the presence and concentration of elements, as well as their oxidation state, coordination number and/or local crystal structure. Previous work has shown that XANES spectroscopy is able to distinguish common silicate minerals [8,9].

Until now, repeated efforts to study insulating samples, maintain constant sample voltage, and extract photoelectrons under X-ray illumination, have yielded modest results. Charging effects on X-PEEM images and spectroscopy occurs when depleted surface charge cannot be compensated in insulating specimen [10].

We specifically addressed this limit and developed a charge compensation approach that guarantees a stable voltage, and high photoelectron yield from the sample surface.

Coating insulating samples with a conductive layer of metal is one obvious solution [11]. However, the escape depth for secondary electrons is on the order of 15–150 Å (at 80–900 eV photon energies) [12]. This limits the thickness of the coating layer.

A maximum coating thickness of 10 Å is mandatory, if the electrons collected by the X-PEEM are to originate from the sample, not from

the coating metal alone. Such a thin metal layer is not sufficient to establish the stable electrical contacts necessary to keep the sample at high voltage. We optimized a differential-thickness coating method that enabled us to analyze thick insulators such as glass slides or minerals embedded in epoxy resin.

The use of X-PEEM in mineral analysis is particularly attractive because it is non-destructive, gives high spatial resolution and chemical sensitivity down to a few tens of nanometers, and can easily image the mineral surface to identify the relevant regions to analyze. Inclusions in polished minerals can be identified while navigating on the sample at low magnification, and detailed high-resolution analysis is done after zooming in to smaller fields of view. While silicate minerals are an excellent test of this approach, the differential-thickness coating will allow X-PEEM analysis of any kind of insulating surface. Sample flatness is a requirement. We do not have accurate measurements of surface roughnesses that we can or cannot observe with X-PEEM. However, we recently tested the sputter coating approach on 20 μm diameter cells with a relief at the edges and the center of the cells of approximately 200 nm and 2 μm from the underlying silicon wafer, respectively, without major image distortion. In the presence of sharp edges, however, the X-PEEM imaging capability rapidly degrades.

2. Differential-thickness coating

The method we developed for charge compensation is summarized in the schematic of Fig. 1. A 10 Å Pt/Pd layer is deposited at the center of the

Fig. 1. Schematic side view of zircons (dark gray) embedded in epoxy (light gray), for X-PEEM analysis (not to scale). The region to be imaged (center) is sputter-coated with 10 Å Pt/Pd (black). Electrical contact is made at the edges, where the Pt/Pd coating is 500 Å thick.

sample, where the X-PEEM imaging and analysis will take place, while a 500 Å thick layer of Pt/Pd is sputter coated around the edges, where the electrical contact is to be made.

The deposition of Pt/Pd (80% platinum, 20% palladium) was performed by magnetron sputtering (manufacturer: Cressington, UK) at room temperature, in 1.5×10^{-2} Torr argon atmosphere and with a 40 mA current. The thickness of the Pt/Pd coating was monitored by a quartz crystal thickness monitor that has a thickness sensitivity of 0.1 Å. The deposition rate was 10 Å/s for the thick edges and 0.1 Å/s for the thin center. The choice of conductive layer and deposition method affect film quality. Sputter deposition of Pt/Pd produces a continuous coating, even on slightly rough or cracked surfaces, which is ideal for enhancing surface conductivity, particularly at low coating thickness. In our experience, pure Pt is completely equivalent to Pt/Pd. While Cr would also give continuous coverage, air exposure is unavoidable when transferring the sample from the sputter chamber to the X-PEEM. The consequent surface oxidation of Cr increases the coating thickness, reducing the yield of electrons from the sample beneath. Pt and Pt/Pd do not significantly oxidize, and are therefore the best coating materials. Gold deposition is not suitable to enhance surface conductivity because it forms discontinuous islands at 10 Å thickness.

3. The sample

The sample of Fig. 1 contains more than 50 zircon ($ZrSiO_4$) crystals from the Jack Hills (Western Australia), including one, studied here, that was previously dated to be the oldest known mineral to have formed on Earth: 4.4 Ga (billion years) old [13,14]. The zircons, ranging in size between 50 and 300 μm, were embedded in a disk of epoxy resin (25 mm diameter, 7 mm thick) then polished with diamond powder down to 0.1 μm in diameter. Following cleaning in ultrasonic baths with ethanol and then distilled water, we sputter coated the polished flat surface (top surface in Fig. 1) as described above. The sample was then transferred to our X-PEEM, SPHINX (Spectro-

microscope for the PHotoelectron Imaging of Nanostructures with X-rays [15]), at the University of Wisconsin–Madison Synchrotron Radiation Center (SRC). For the test described below SPHINX was mounted on the HERMON (High Energy Resolution MONochromator, 62–1200 eV) beamline, and the sample was imaged and analyzed at the Si L edge, while kept at a potential of −20 kV, base pressure of 10^{-10} Torr and room temperature.

4. Zircon inclusions

Inclusions in minerals are indicative of the environment and conditions of mineral formation, and subsequent history. We have studied a number of detrital zircon crystals from metaconglomerate in the Jack Hills [13,14] with the aim of identifying silicate inclusions, which may carry evidence of rocks from which these zircons originated. Many inclusions in these zircons measure 1 μm or less in diameter, and the spatial resolution of X-PEEM enables their analysis. Figs. 2b and c show several inclusions in the 4.4 Ga zircon.

5. X-PEEM microanalysis of inclusions

We present in Fig. 2a the SPHINX micrograph of the entire 4.4 Ga zircon, a zoomed-in micrograph (Fig. 2b) and a visible light micrograph (Fig. 2c) at identical magnification. In Figs. 2b and c the same cracks and inclusions can be recognized. The similarity between the low magnification X-PEEM images and the visible light micrographs proves the efficacy of our coating approach. This sample cannot be imaged in X-PEEM without the conductive overlayer.

We analyzed several inclusions in the 4.4 Ga zircon with the SPHINX instrument. We present in Fig. 3 the Si $L_{2,3}$ XANES spectra of inclusions #1 and #6, and of a zircon region, extracted from SPHINX movies. These spectra are compared with reference spectra acquired previously [8]. Previous electron microprobe analysis (EMPA) and scanning electron microscopy energy dispersive X-ray analysis (SEM-EDX) had established inclusion #1
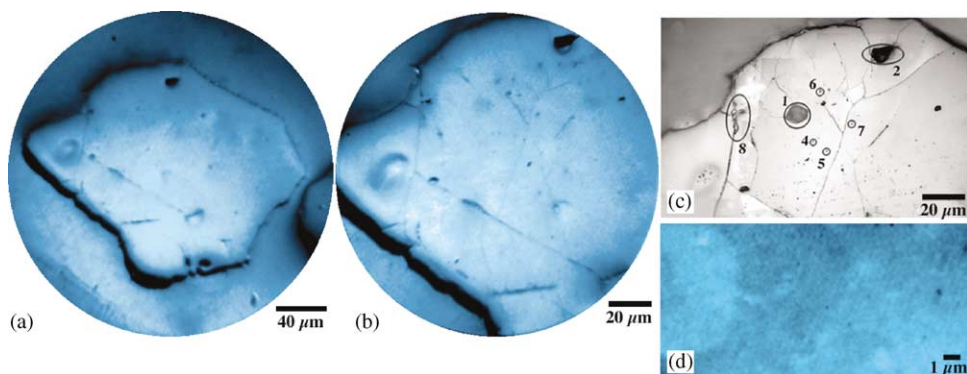
Fig. 2. (a) Lowest magnification SPHINX X-PEEM micrograph of the entire Pt/Pd coated 4.4 Ga zircon W74-2, acquired at 105 eV, (b) low magnification SPHINX micrograph of a portion of the zircon, in which several inclusions are visible, (c) reflectance bright field visible light micrograph of the inclusions, at the same magnification as (b). Inclusions #1, #2 and #8 are large enough to be studied with other microanalytical techniques. Inclusions #4, #5, #6 and #7 can only be studied non-destructively with X-PEEM and differential-thickness coating. The field of view for SPHINX images can be varied continuously between 240 and 1.7 μm and (d) higher magnification SPHINX micrograph (at 130 eV) of inclusion #1 and inclusion #6. These silicate inclusions do not show high contrast with respect to the surrounding zircon silicate. They are better displayed with chemical contrast in Fig. 4.
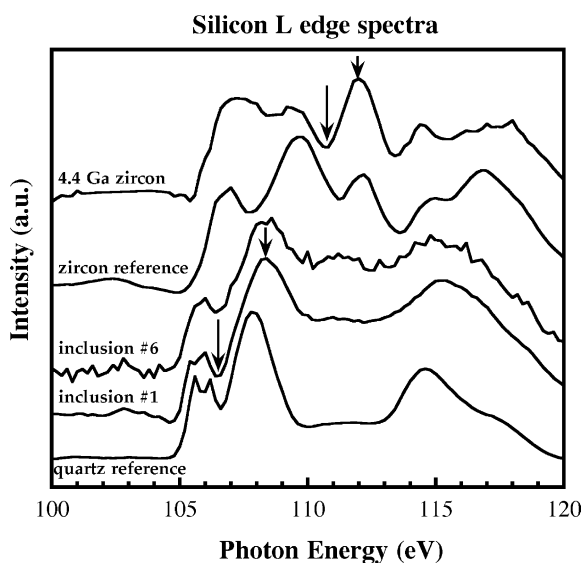
Fig. 3. Si $L_{2,3}$ XANES. From the top: SPHINX spectrum extracted from a region of zircon at the center of Figs. 2d and 4 (2 μm × 2 μm square region); zircon reference spectrum [8]; SPHINX spectrum from inclusion #6 (circular region, 800 nm diameter); SPHINX spectrum from inclusion #1 (2 μm × 3 μm rectangular region); reference quartz spectrum [8]. All spectra were acquired between 90 and 130 eV, and are identically normalized to a 7th order polynomial interpolation to the spectrum, masked in the range 104–120 eV that contains the Si L edge fine structure. Spectra are displaced vertically for clarity. The arrows indicate the energies of the on-peak and off-peak images used to obtain the maps in Fig. 4.

to be pure SiO_2 but could not distinguish amongst the polymorphs of SiO_2: quartz, tridymite, cristobalite, coesite or stishovite. These minerals have different crystal structures that can be distinguished by XANES [16].

The XANES spectrum from this inclusion is in agreement with the quartz reference. The composition of inclusion #6 was discovered only when a distribution map for quartz was created, using the procedure described below. We also obtain good agreement with the XANES spectrum from this region and a quartz reference mineral. Inclusion #6 is approximately 800 nm in diameter and could not be analyzed by SEM-EDX, EMPA or Raman spectroscopy.

We present in Fig. 4 the silicates distribution maps of the zircon with inclusions #1 and #6. As both quartz (SiO_2) and zircon ($ZrSiO_4$) are silicate minerals (SiO_4 tetrahedra), the Si oxidation state and coordination number are identical. Hence their differing spectral line shape originates from the different crystal structures (Si–O bond angles) and orbital overlap with the Zr cation. There exist several numerical methods of mapping species associated with known XANES line shape [17–19], although simple image processing allows regions of zircon and quartz to be distinguished. We used image ratios to obtain spatially resolved maps of
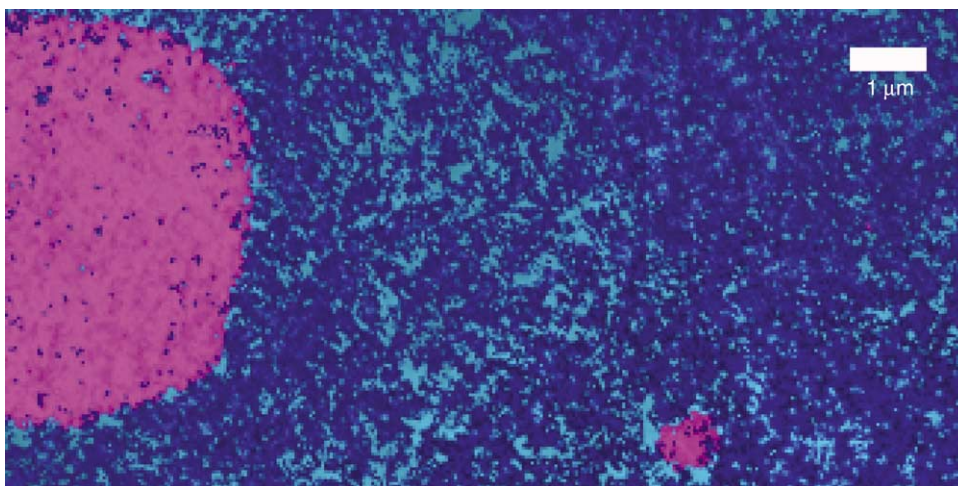
Fig. 4. Distribution maps of quartz (magenta) and zircon (blue), extracted from SPHINX XANES movies, acquired on the same sample region as Fig. 2d and superimposed on the direct image of Fig. 2d (cyan). The inclusion on the left is #1, the smaller one on the right is #6 (as labeled in Fig. 2c).

the two minerals by selecting, with reference to the spectra in Fig. 3, photon energies that maximize the contrast. The maps of Fig. 4 represent the best result.

Distribution maps of zircon and quartz were obtained by digital ratio of two images, on-peak and off-peak, at photon energies chosen to highlight quartz or zircon. The quartz map was obtained by digital ratio of two images acquired at 108.4 and 106.4 eV photon energy. The zircon map is the ratio of images at 112.0 and 110.4 eV. This procedure is not quantitative, but allows rapid and accurate display of the spatial distribution of the silicate species. The results of the mapping were verified by ensuring that spectra extracted from highlighted areas were indeed in agreement with the reference spectra. The two distribution maps were converted to color and fused with Adobe Photoshop 7.

The spectra from inclusions #6 and #1 (Fig. 3) are very similar in line shape, while the noise level is greater for #6, since the acquisition region is smaller. Note that spectra can be extracted from a single pixel in a movie. In the present case, the pixel size was 50 nm, but we have acquired spectra from 35 nm pixels in other zircons [8]. For the latter work, SPHINX was mounted on a 6 m TGM beamline, optimized for flux and not for resolution as in the case of the HERMON beamline.

Sub-micron spatial mapping of silicate species demonstrates the potential of combining the high chemical sensitivity of XANES spectroscopy with high-resolution imaging. The limit for spatially resolving chemical species in X-PEEM varies with element and absorption edge, but is presently determined by the signal at high magnification, not the imaging optics of the X-PEEM [20–22]. Improved signal quality, and hence higher chemical resolution is possible when studying elements that have core absorption edges at higher binding energies than the Si L edge around 100 eV. The increase in secondary electron escape depth with photon energy implies that a greater signal is obtained from the sample through the conductive overlayer. Increasing the number of photons per unit area per unit time available on the beamline will enhance the performance for all elements studied. The SRC is currently developing an undulator beamline optimized for spectromicroscopy that will offer 10^{13} photons/s, in a 20 μm × 80 μm spot size, and 100–1800 eV energy range, with a modest resolving power $E/\Delta E \sim 1000$, which is adequate for X-ray absorption spectra. With this beamline, at the beginning of 2004, we will be able to analyze the chemistry of minerals

and other thick insulators with better than 20 nm resolution.

6. Conclusions

We tested a new differential coating technique to analyze insulating samples with X-PEEM. The SPHINX X-PEEM images, spectra and distribution maps demonstrate the effectiveness of this approach. We observed an 800 nm diameter quartz inclusion in a 4.4 Ga old zircon fragment, and identified it as quartz. Such an inclusion is too small to be analyzed with any other non-destructive technique currently available to mineralogists. With the complete removal of charging, the samples that can be analyzed by X-PEEM include insulators and conductors, even of significant thickness. The only stringent limitations still outstanding are UHV compatibility and surface flatness.

References

[1] A. Scholl, J. Stöhr, J. Lüning, J.W. Seo, J. Fompeyrine, H. Siegwart, J.-P. Locquet, F. Nolting, S. Anders, E.E. Fullerton, M.R. Scheinfein, H.A. Padmore, Science 287 (2000) 1014.

[2] J. Stöhr, Y. Wu, B.D. Hermsmeier, M.G. Samant, G.R. Harp, S.F. Koranda, D. Dunham, B.P. Tonner, Science 259 (1993) 658.

[3] W. Engel, M.E. Kordesh, H.H. Rotermund, S. Kubala, A. von Oertzen, Ultramicroscopy 36 (1991) 148.

[4] G. De Stasio, P. Casalbore, R. Pallini, B. Gilbert, F. Sanità, M.T. Ciotti, G. Rosi, A. Festinesi, L.M. Larocca, A. Rinelli, D. Perret, D.W. Mogk, P. Perfetti, M.P. Mehta, D. Mercanti, Cancer Res. 61 (2001) 4272.

[5] M. Labrenz, G.K. Druschel, T. Thomsen-Ebert, B. Gilbert, S.A. Welch, K.M. Kemner, G.A. Logan, R.E. Summons, G. De Stasio, P.L. Bond, B. Lai, S.D. Kelly, J.F. Banfield, Science 290 (2000) 1744.

[6] N. Metrich, M. Bonnin-Mosbah, J. Susini, B. Menez, L. Galoisy, Geophys. Res. Lett. 29 (2002) 33-1.

[7] Z. Cai, B. Lai, W. Yun, I. McNulty, A. Khounsary, J. Maser, P. Ilinski, D. Legnini, E. Trakhtenberg, S. Xu, B. Tieman, G. Wiemerslage, E. Gluskin, AIP Conf. Proc. 521 (2000) 31.

[8] B. Gilbert, B.H. Frazer, F. Naab, J. Fournelle, J.W. Valley, G. De Stasio, Am. Mineral. 88 (2003) 763.

[9] L.A.J. Garvie, P.R. Busek, Am. Mineral. 84 (1999) 946.

[10] B. Gilbert, R. Andres, P. Perfetti, G. Margaritondo, G. Rempfer, G. De Stasio, Ultramicroscopy 83 (2000) 129.

[11] B. Gilbert, G. Margaritondo, S. Douglas, K.H. Nealson, R.F. Egerton, G. Rempfer, G. De Stasio, J. Electron Spectrosc. Relat. Phenom. 114 (2001) 1005.

[12] B.H. Frazer, B. Gilbert, B.R. Sonderegger, G. De Stasio, Surface Sci., in press.

[13] S.A. Wilde, J.W. Valley, W.H. Peck, C.M. Graham, Nature 409 (2001) 175.

[14] J.W. Valley, W.H. Peck, E.M. King, S.A. Wilde, Geology 30 (2002) 351.

[15] B.H. Frazer, M. Girasole, L.M. Wiese, T. Franz, G. De Stasio, Rev. Sci. Instr., submitted for publication.

[16] D. Li, G.M. Bancroft, M. Kasrai, M.E. Fleet, R.A. Secco, X.H. Feng, K.H. Tan, B.X. Yang, Am. Mineral. 79 (1994) 622.

[17] C.J. Buckley, N. Khaleque, S.J. Bellamy, M. Robins, X. Zhang, J. Phys. IV 7 (C2 Part 1) (1997) 83.

[18] I.N. Koprinarov, A.P. Hitchcock, C. McCrory, R.F. Childs, J. Phys. Chem. B 106 (2002) 5358.

[19] B.H. Frazer, B.R. Sonderegger, B. Gilbert, K.L. Richter, C. Salt, L. Wiese, D. Rajeshf, S.P. Howard, J.F. Fowler, M.P. Mehta, G. De Stasio, Proceedings of the 2002 X-ray Microscopy Conference, J. Phys. IV 104 (2003) 349.

[20] G. De Stasio, L. Perfetti, B. Gilbert, O. Fauchoux, M. Capozi, P. Perfetti, G. Margaritondo, B.P. Tonner, Rev. Sci. Instr. 70 (1999) 1740.

[21] G. De Stasio, B. Gilbert, B.H. Frazer, T. Franz, C. Koziol, E. Bauer, 12th US National Synchrotron Radiation Instrumentation Conference, Madison, WI, August 22–24, 2001, Abstract Book.

[22] S. Anders, H.A. Padmore, R.M. Duarte, T. Renner, T. Stammler, A. Scholl, M.R. Scheinfein, J. Stöhr, L. Séve, B. Sinkovic, Rev. Sci. Instr. 70 (1999) 3973.